Structural Engineering and Mechanics, Vol. 7, No. 2 (1999) 225-240
DOI: http://dx.doi.org/10.12989/sem.1999.7.2.225

Viscoelastic constitutive modeling of asphalt concrete with growing damage

Hyun-Jong Lee†

Department of Civil Engineering, Kangnung National University, Kangnung 210-702, Korea

Y. Richard Kim‡

Department of Civil Engineering, North Carolina State University, Raleigh, NC 29695-7908, U.S.A.

Sun-Hoon Kim†

Department of Civil Engineering, Youngdong University, Chungbuk 370-800, Korea

Abstract. This paper presents a mechanistic approach to uniaxial viscoelastic constitutive modeling of asphalt concrete that accounts for damage evolution under cyclic loading conditions. An elastic-viscoelastic correspondence principle in terms of pseudo variables is applied to separately evaluate viscoelasticity and time-dependent damage growth in asphalt concrete. The time-dependent damage growth in asphalt concrete is modeled by using a damage parameter based on a generalization of microcrack growth law. Internal state variables that describe the hysteretic behavior of asphalt concrete are determined. A constitutive equation in terms of stress and pseudo strain is first established for controlled-strain mode and then transformed to a controlled-stress constitutive equation by simply replacing physical stress and pseudo strain with pseudo stress and physical strain. Tensile uniaxial fatigue tests are performed under the controlled-strain mode to determine model parameters. The constitutive equations in terms of pseudo strain and pseudo stress satisfactorily predict the constitutive behavior of asphalt concrete all the way up to failure under controlled-strain and -stress modes, respectively.

Key words: asphalt concrete; correspondence principle; constitutive model; cyclic test; damage; fatigue; viscoelasticity.

1. Introduction

Fatigue cracking due to repeated traffic loading is one of the major distresses in asphalt concrete pavements. Accurate prediction of the fatigue performance of these pavements requires understanding of the hysteretic behavior of asphalt concrete under realistic traffic conditions.

The hysteretic behavior of asphalt concrete under traffic loading is attributed to three major mechanisms (Kim and Little 1990, Lee and Kim 1997): damage growth; relaxation of stresses in

† Assistant Professor
‡ Associate Professor

the system due to the viscoelasticity of asphalt concrete; and microcrack healing. Since these three mechanisms take place simultaneously, it is important to model the damage growth separately from the viscoelastic effect to simplify the modeling of the mechanical behavior of asphalt concrete.

Kim and Little (1990) applied the correspondence principle (Schapery 1984) to transform the viscoelastic analysis to an elastic case. A time-dependent damage parameter based on the microcrack growth law (Schapery 1981) was then employed to model the damage growth in asphalt concrete. The resulting constitutive model satisfactorily predicted the hysteretic behavior of sand-asphalt under the controlled-strain mode (Chan *et al.* 1994). In this study, the same methodology was used to model the constitutive behavior of asphalt concrete.

Although Kim and Little (1990) successfully modeled the short-term fatigue damage evolution of sand-asphalt, the materials and testing conditions were less representative of the field conditions. In this study, therefore, more realistic conditions were used in the modeling to increase the applicability of the model to actual pavement design and analysis. The major difference in this study from Kim and Little (1990) is the fact that the mode-of-loading effects and long-term fatigue damage evolution of asphalt concrete are included in the constitutive modeling.

In general, fatigue test methods fall into one of two types (Mattos and Sampaio 1995), either *controlled-stress* when a constant stress amplitude is applied, or *controlled-strain* when a constant strain amplitude is applied. The controlled-stress mode of loading appears to represent the response of thick asphalt pavements to repetitive loading, while the controlled-strain approach is suitable for thin pavements (Yoder and Witczak 1975). The controlled-strain mode of testing results in a greater fatigue life for the same mixture than the controlled-stress testing.

It is the authors' belief that a true material model should be independent of the mode of loading because the material does not know which mode it is subjected to. That is, the material simply responds when it is loaded. A model of fatigue behavior that is independent of the mode of loading, which is neither controlled-stress nor controlled-strain, would be a substantial improvement over existing models, and would results in more realistic predictions of fatigue life of asphalt pavements.

2. Constitutive theory

2.1. Correspondence principle (CP)

Schapery (1984) proposed the extended elastic-viscoelastic correspondence principle which can be applicable to both linear and nonlinear viscoelastic materials. He suggested that constitutive equations for certain viscoelastic media are identical to those for the elastic cases, but stresses and strains are not necessarily physical quantities in the viscoelastic body. Instead, they are pseudo variables in the forms of convolution integral such that:

$$\varepsilon^R = \frac{1}{E_R}\int_0^t E(t-\tau)\frac{\partial \varepsilon}{\partial \tau}\,d\tau \tag{1}$$

$$\sigma^R = E_R\int_0^t D(t-\tau)\frac{\partial \sigma}{\partial \tau}\,d\tau \tag{2}$$

where ε^R and σ^R are uniaxial pseudo strain and pseudo stress, respectively. E_R is reference

modulus that is an arbitrary constant, and $E(t)$ and $D(t)$ is uniaxial relaxation modulus and creep compliance, respectively.

Depending upon the traction boundary conditions, a viscoelastic problem can be transformed to an elastic problem using σ and ε^R or σ^R and ε. For instance, a uniaxial stress-strain relationship for linear viscoelastic materials is:

$$\varepsilon=\int_0^t D(t-\tau)\frac{d\sigma}{d\tau}d\tau \tag{3}$$

Using the definition of pseudo stress in Eqs. (2) and (3) can be rewritten as:

$$\sigma^R=E_R\varepsilon \tag{4}$$

A correspondence can be found between Eq. (4) and a linear elastic stress-strain relationship.

2.2. Damage parameter

For viscoelastic materials, Schapery (1984) showed that the local crack growth rate (da/dt) obeys a power law in local J integral,

$$\frac{da}{dt}=A(J_v)^k \tag{5}$$

where J_v is generalized J integral; and A and k are positive constants. According to the theory, the exponent k is a function that depends on characteristics of a failure zone. For example, if the material's fracture energy (Γ) and failure stress within the fracture process zone are constants, then k=1+1/m, where m is the exponent of creep compliance versus time in the power law relationship. If the fracture process zone size and Γ are constants, k=1/m.

The final form of the damage parameter based on the generalization of the microcrack growth law is:

$$S_p=\left(\int_0^t|\sigma^{\frac{1}{N}}|^p\,dt\right)^{\frac{1}{p}} \tag{6}$$

where p=(1+N) k, and $\sigma\propto|\varepsilon^R|^N$. This damage parameter S_p represents damage state in the body due to microcrack propagation.

To predict strains from known stresses, the damage parameter based on stress in Eq. (6) is useful. However, if the strains are known, the following damage parameter based on pseudo strain is recommended:

$$S_p=\left(\int_0^t|\varepsilon^R|^p\,dt\right)^{\frac{1}{p}} \tag{7}$$

This form is known as a Lebesgue norm of ε^R. When p goes to infinity (i.e., for elastic materials), S_p becomes the largest absolute value of pseudo strain up to the current time, denoted here by $|\varepsilon_L^R|$ (Reddy and Rasmussen 1982).

3. Materials and testing programs

All specimens were fabricated using Watsonville granite aggregate and AAD and AAM asphalt

cements used in the Strategic Highway Research Program (hereinafter, denoted as AAD and AAM mixtures, respectively). In this paper, only AAD mixture data are presented, and AAM mixture data can be found in Lee (1996). Aggregates were mixed by a mechanical mixer with 5.0% asphalt cement by weight of dry aggregate at 140°C for four minutes. The mixture was compacted in a rectangular mold at 116°C by a rolling wheel compactor and cured at room temperature for two days before coring 102 mm (4 inches) diameter by 203 mm (8 inches) height cylindrical specimens from the slab. The specimens were cored in a horizontal direction perpendicular to the compaction force applied, consistent with the direction of tensile stress and/or strain developed near the bottom of an asphalt concrete layer in actual pavement systems.

All tests were conducted in a uniaxial tension mode using a servo-hydraulic closed-loop-testing machine. For the characterization of viscoelastic properties of the materials, three different types of tests, such as creep, relaxation, and dynamic modulus tests, were conducted at various temperatures. To study the applicability of CP to the materials used in this study, controlled-stress cyclic loading tests at relatively low stress amplitude were conducted, and constant-strain-rate monotonic loading tests with varying strain rates were performed. The controlled-stress and -strain cyclic loading tests with various stress and strain amplitudes were conducted at 25°C to develop a constitutive model for asphalt concrete. A haversine wave with 0.1-second loading time was used in cyclic loading. Stresses and strains used in the analysis were nominal (average) values.

4. Mechanical properties of asphalt mixture

Creep and relaxation tests were performed on several specimens at −5, 5, 15, 25, and 33°C to obtain master creep compliance and master relaxation modulus curves as shown in Fig. 1. The individual creep compliance-time curves at different temperatures were used to construct the master creep curve at the reference temperature of 25°C. The following Prony series representation was used to analytically represent the master creep curve:

$$D(\xi)=D_0+\sum_{i=1}^{M} D_i\left(1-e^{-\frac{\xi}{\tau_i}}\right) \tag{8}$$

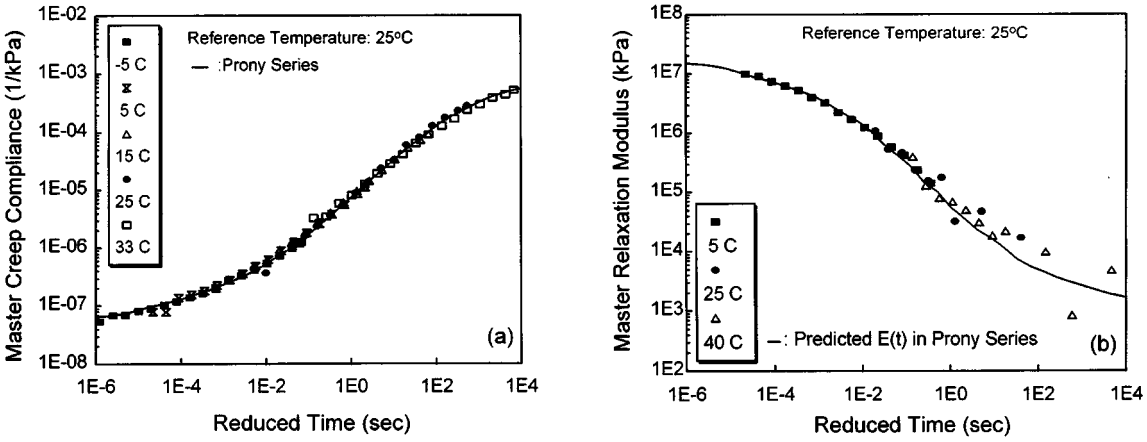

Fig. 1 Creep and relaxation master curves at a reference temperature: (a) creep master curve; (b) relaxation master curve

where $D(\xi)$ = master creep compliance in 1/kPa,
ξ = reduced time,
τ_i = retardation time of the ith Voigt element, and
D_0, D_i = material constants.

The model constants in Eq. (8) can be found by minimizing the square error between the measured creep data and the analytical representation. The τ_i may be specified in many different ways and normally be separated by no more than one decade to obtain a smooth curve.

Calculation of pseudo strain requires the expression of relaxation modulus as a function of time. The relaxation test is fairly cumbersome to perform because the immediate increase in strain input results in a large initial load response. For practical purposes, it is desirable to predict the relaxation modulus from a simpler test, such as the creep test (Kim *et al.* 1995).

Based on the linear viscoelastic theory, relaxation moduli were predicted from the creep compliance values, and plotted with the measured values in Fig. 1(b). Generally a good match is observed between the predicted and measured data, although the fit becomes poorer at times longer than 10 seconds because of the limitation in data acquisition resolution and the effect of logarithmic scale. For the remainder of the analysis in this paper, the relaxation modulus predicted from the creep test is used.

To analytically represent the master relaxation curve presented in Fig. 1(b), the following Prony series representation was used:

$$E(\xi)=E_\infty+\sum_{i=1}^{M} E_i(e^{-\frac{\xi}{\rho_i}}) \tag{9}$$

where $E(\xi)$ = master relaxation modulus in kPa, E_∞ is long-time equilibrium modulus, E_i's are regression constants, and ρ_i's are relaxation times.

In the calculation of pseudo variables for cyclic loading, which will be discussed in the following section, the absolute values of complex modulus $|E^*|$ or complex compliance $|D^*|$ is required. First, based on the linear viscoelastic theory, $|E^*|$ values were predicted from $D(t)$. $|D^*|$ values were then determined from the following relationship:

$$E^* \times D^* = 1 \tag{10}$$

An analytical procedure for the conversion of $D(t)$ to $|E^*|$ or $|D^*|$ was established in this study, and detailed discussion involved in this analysis can be found in Lee (1996).

In order to validate the conversion scheme established in this study, dynamic modulus tests were conducted at three different temperatures with varying frequencies. Using individual dynamic modulus curves at various temperatures, the master dynamic modulus curves were constructed at the reference temperature of 25°C and presented in Fig. 2. Also the dynamic moduli were predicted from $D(t)$ values given in Fig. 1(a), and illustrated as the continuous line in this figure. In general, a good agreement between the measured and predicted moduli is found, which proves the validity of the conversion procedure established in this study.

5. Calculation of pseudo variables

Pseudo strain or pseudo stress is an essential parameter for applying Schapery's correspondence principle (1984) to the hysteretic stress-strain behavior of asphalt concrete. As shown in Eq. (1),

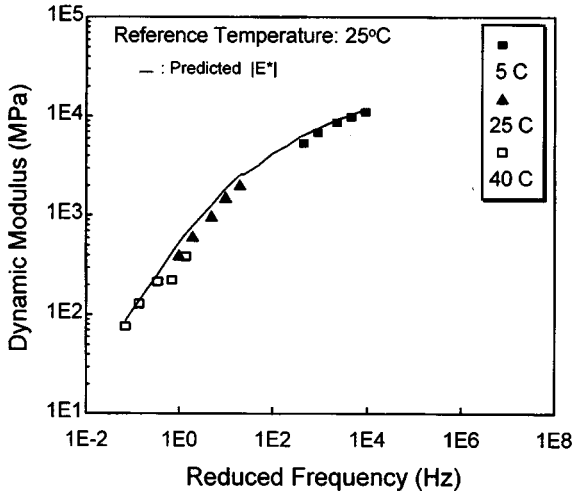

Fig. 2 Master dynamic modulus curve at a reference temperature

the computation of the pseudo strain requires the acquisition of strain values from time zero to time t. This method is impractical to be used in the long-term fatigue analysis due to limitations in computer memory capacity and computing time. An alternate way to calculate the pseudo strain is to present the relaxation modulus and the strain as analytical functions of time and integrate the product of these functions.

In the controlled-strain mode, the haversine strain history can be simply represented in an analytical function as follows:

$$\varepsilon(t)=[\varepsilon_0+\varepsilon_0\sin(\omega t+\theta)]H(t) \tag{11}$$

where ε_0 is a strain amplitude, ω is an angular velocity of strain input, t is a current time, θ is a regression constant, and $H(t)$ is heaviside step function such that H=0 when t<0, and H=1 when t>0. From Eqs. (1) and (11), we can obtain

$$\varepsilon^R(t)=\frac{1}{E_R}[\varepsilon_0 E(t)+\varepsilon_0|E^*|\sin(\omega t+\theta+\phi)] \tag{12}$$

where ϕ is a phase angle, $E(t)$ is the uniaxial relaxation modulus given in Eq. (9).

Similarly, the stress input and pseudo stress response are represented as follows:

$$\sigma(t)=[\sigma_0+\sigma_0\sin(\omega t+\theta)]H(t) \tag{13}$$

$$\sigma^R(t)=E_R[\sigma_0 D(t)+\sigma_0|D^*|\sin(\omega t+\theta+\phi)] \tag{14}$$

where σ_0 is a stress amplitude. More detailed steps involved in deriving Eqs. (12) and (14) can be found in Lee (1996). For the simplicity of analysis, E_R=1.0 was used in all the calculations of pseudo variables.

6. Constitutive modeling of asphalt concrete

6.1. Experimental study of CP

Prior to constitutive modeling, the material's behavior was studied with the application of the

CP. The types of uniaxial tensile testing used were as follows:

1. Controlled-stress cyclic loading tests; and
2. Constant-strain-rate monotonic loading tests with varying strain rates.

In the cyclic loading tests, loading amplitude of 156N (35 lbs) was used, which was low enough not to induce any significant damage. Typical hysteretic stress-strain behavior is presented in Fig. 3(a) at selected cycles. As expected, the stress-strain loops shift to the right-hand side with the reduction of dissipated energy determined from the area inside the stress-strain curve. In Fig. 3(b), the same strains are plotted against pseudo stresses calculated based on Eq. (14). As can be seen from Figs. 3(a) and 3(b), hysteretic behavior due to both loading-unloading and repetitive loading has disappeared using the pseudo stresses. It is also noted that the pseudo stress-strain behavior in Fig. 3(b) is linear. Lee and Kim (1997) observed a similar result employing pseudo strain instead of pseudo stress.

In the monotonic loading tests, four different strain rates ranging from 0.00005 to 0.0032 units/second were used. Fig. 4(a) displays the rate-dependent behavior observed from AAD mixture. Pseudo strains were plotted against σ/I in Fig. 4(b). The initial pseudo stiffness I, defined as the

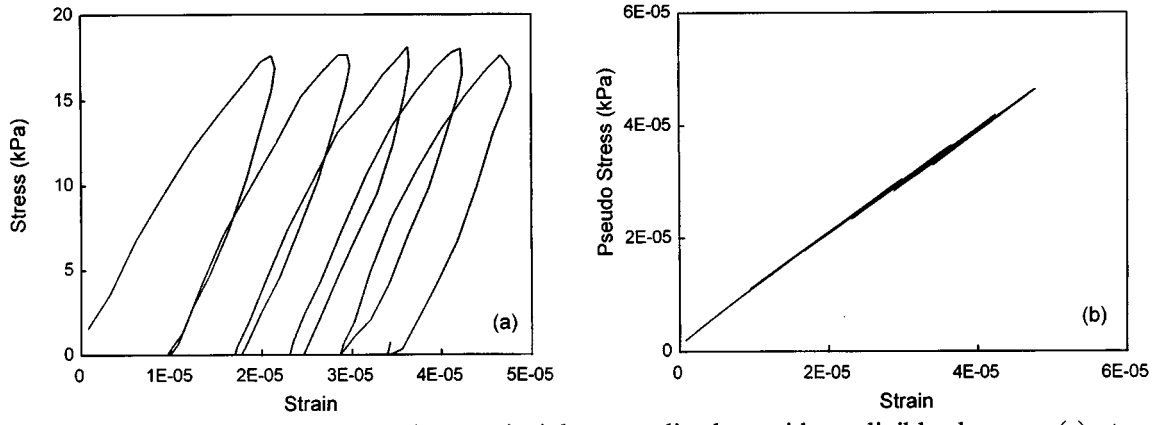

Fig. 3 Application of the correspondence principle to cyclic data with negligible damage: (a) stress-strain; (b) pseudo stress-strain

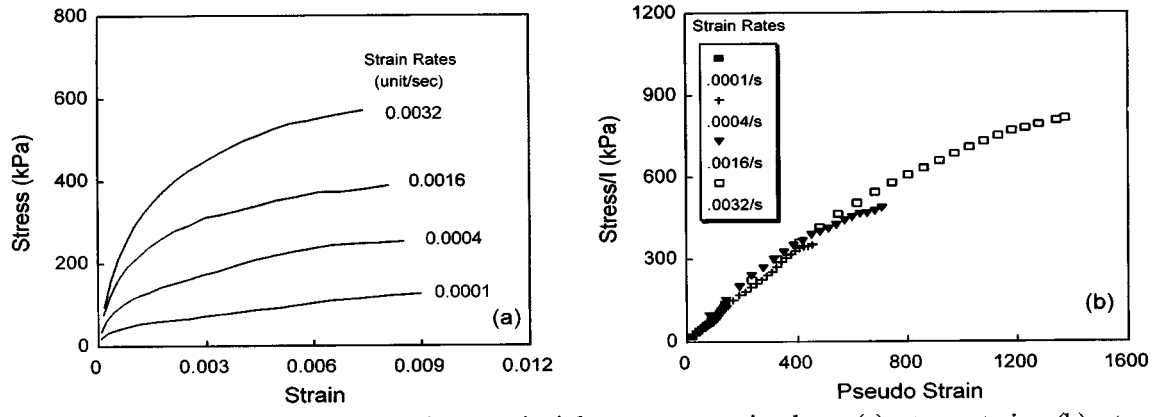

Fig. 4 Application of the correspondence principle to monotonic data: (a) stress-strain; (b) stress-pseudo strain

ratio of stress to pseudo strain at the early linear part of a stress-pseudo strain curve, was necessary to reduce the effect of sample-to-sample variability. The curves representing different loading rates fall on the same line at lower stress levels, and then the discrepancy in the stress-pseudo strain curves among the different loading rates becomes greater. This behavior implies that the correspondence principle can successfully eliminate the rate dependency of the material when the damage is negligible. However, if a significant level of damage is induced in the sample, additional variables should be employed in a constitutive equation to represent the damage growth in the system.

6.2. Uniaxial viscoelastic constitutive model under the controlled-strain mode

Since a linear relationship between the stress and pseudo strain has been found when the damage was negligible in the proceeding section, it was assumed that the material was linearly viscoelastic and that any deviation from the linear viscoelastic behavior was due to damage. Thus, the following form of the constitutive model was employed in this study:

$$\sigma = I(\varepsilon^R) D(S_m) \tag{15}$$

where I=initial pseudo stiffness, $D(S_m)$=damage function, and S_m=internal state variables (ISV).

To study the damage growth in asphalt concrete, the controlled-strain fatigue tests were conducted with two strain amplitudes. These strain levels were high enough to induce some damage to the specimens. Fig. 5 shows typical stress-pseudo strain hysteresis loops at different numbers of cycles. Different from the negligible damage case in Fig. 3(b), the loading and unloading paths in each cycle are nonlinear due to the damage. In addition, the stiffness reduction of the material due to damage growth results in the change of the slope of each cycle as cyclic loading continues. To represent this change of the slope, *secant pseudo stiffness*, denoted by S^R, was defined as the ratio of a stress value to a pseudo strain value at the peak pseudo strain of each cycle.

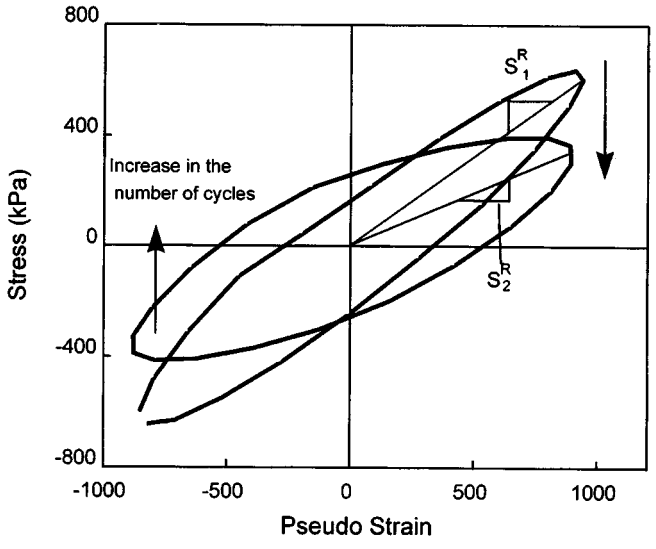

Fig. 5 Stress-pseudo strain behavior of asphalt concrete under controlled-strain cyclic loading

As can be seen from the loading and unloading curves in Fig. 5, there are two different stresses associated with one ε^R value. On the loading path, the stress is a function of current ε^R only, while on the unloading path, the stress is a function of current ε^R and the largest ε^R during the ε^R history up to that time ($\varepsilon_L{}^R$). This observation suggests the use of $\varepsilon^R/\varepsilon_L{}^R$ in identifying whether the point of interest is on the loading path or on the unloading path (Kim and Little 1990). That is, $\varepsilon^R/\varepsilon_L{}^R=1$ during the loading path, and $\varepsilon^R/\varepsilon_L{}^R<1$ during the unloading path. Therefore, Eq. (15) becomes:

$$\sigma=I(\varepsilon^R)D\left(\frac{\varepsilon^R}{\varepsilon_L^R}, S_m\right) \tag{16}$$

where $m=2, 3, \cdots, M$.

It was found from the experimental data that the size of each stress-pseudo strain hysteresis loop was dependent upon the stress amplitude incurred in a specimen. That is, the larger the stress amplitude, the bigger the hysteresis loop. Since the stress is the parameter to be predicted from the constitutive equation and $\sigma \propto |\varepsilon^R|^N$, the amplitude of pseudo strain, denoted by $\varepsilon_0{}^R$, is selected as another ISV to represent the effect of the stress amplitude on the hysteresis loops:

$$\sigma=I(\varepsilon^R)D\left(\frac{\varepsilon^R}{\varepsilon_L^R}, \varepsilon_0^R, S_m\right) \tag{17}$$

where $m=3, 4, \cdots, M$.

Although $\varepsilon^R/\varepsilon_L{}^R$ and $\varepsilon_0{}^R$ are sufficient to model the hysteretic behavior in each cycle, another ISV is needed to model the change in the slope of each cycle as cyclic loading continues. Knowing the reduction in this slope is related to the fatigue crack growth, the damage parameter S_p is employed in the constitutive model as another ISV. Thus Eq. (17) becomes:

$$\sigma=I(\varepsilon^R)D\left(S_p, \frac{\varepsilon^R}{\varepsilon_L^R}, \varepsilon_0^R\right) \tag{18}$$

To obtain the explicit form of the damage function D, several forms of the constitutive model were attempted using the experimental data, and the following additive form was found to yield the best result:

$$\sigma=I(\varepsilon^R)\left[F(S_p)+G\left(\varepsilon_0^R, \frac{\varepsilon^R}{\varepsilon_L^R}\right)\right] \tag{19}$$

The function F represents the change in the secant pseudo stiffness (S^R) during cyclic loading, and the function G accounts for the hysteretic behavior of stress-pseudo strain relationship.

6.3. Characterization of the material functions F and G

In order to calculate S_p, the parameter p should be determined a priori. In this study, it is assumed that the material is linearly viscoelastic (i.e., $N=1$). If so, as discussed earlier, the value

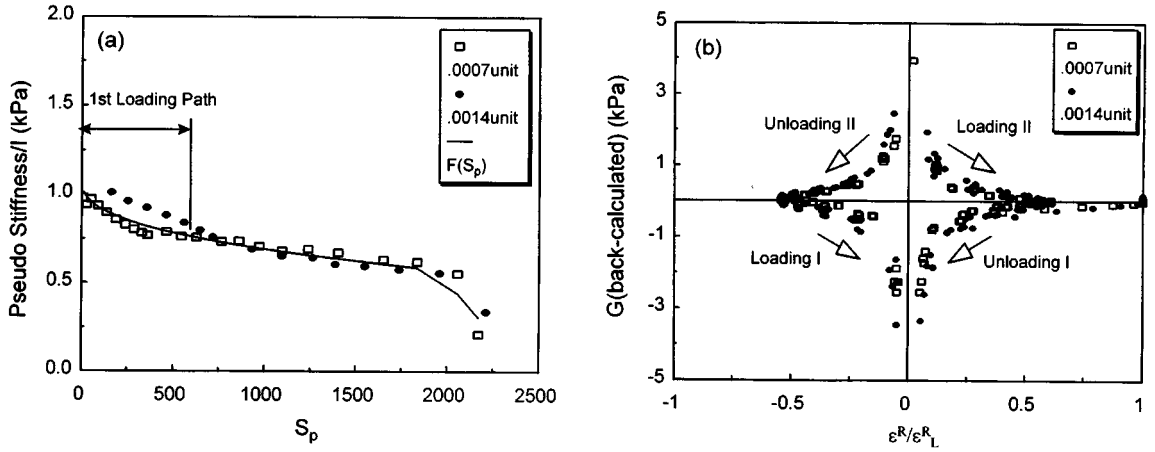

Fig. 6 Damage evolution in asphalt concrete under the controlled-strain mode: (a) S^R vs S_p; (b) back-calculated G vs $\varepsilon^R/\varepsilon_L^R$

of p is equal to $2(1+1/m)$ or $2/m$ depending upon the characteristics of the failure zone. Based on earlier work (Kim and Little 1990), $p=2(1+1/m)$ was assumed. Typical m value obtained from the creep tests were 0.628, which results in a p value of 5.19.

In Fig. 6(a), S^R/I was plotted against S_p determined from Eq. (7). The data presented in this figure includes the data from the entire loading path of the first cycle and the values of the remaining cycles up to failure. The discrepancies between two strain-level data in the first loading path could be due to experimental errors where some minor adjustments occur within the test setup. However, after the first loading path, all the data from two different strain amplitudes fall on the same curve up to failure. Since the same loading time (0.1 second) for the two strain amplitudes produced different strain rates for the two tests, S_p demonstrates its ability of accounting for the effect of strain rates on damage growth. The regression analysis on the controlled-strain data resulted in the following equation for the function F:

$$F(S_p)=F_0-F_1(S_p)^{F_2} \tag{20}$$

The regression coefficients in Eq. (20) are presented in Table 1.

To find the explicit form of G, $F(S_p)$ was subtracted from $\sigma/(I\varepsilon^R)$ in Eq. (19) (hereinafter, called back-calculated G) and then plotted against $\varepsilon^R/\varepsilon_L^R$. As shown in Fig. 6(b) and in Eq. (21) below, a strong power relationship was observed between the back-calculated G and $\varepsilon^R/\varepsilon_L^R$. In this figure, the value of $\varepsilon^R/\varepsilon_L^R$ increases during loading (Loading I for the negative values of $\varepsilon^R/\varepsilon_L^R$ and Loading II for the positive values of $\varepsilon^R/\varepsilon_L^R$) while it decreases during unloading (Unloading I for the positive values of $\varepsilon^R/\varepsilon_L^R$ and Unloading II for the negative values of $\varepsilon^R/\varepsilon_L^R$). The study of this data produced the following form of function G:

Table 1 Coefficients in Eq. (20)

F_0	F_1	F_2	Boundary condition
1.008	0.00046	0.93	$S_p \leq 1{,}820$
3.174	0.00146	1.0	$S_p > 1{,}820$

Table 2 Coefficients in Eq. (21) and (22)

Function G				Function G_2		
Boundary condition	G_0	G_1	G_{2R}	Boundary condition	β_0	β_1
$\varepsilon^R/\varepsilon_L^R < 0$, and increases	0.1917	−0.1765	−1.00	$\varepsilon_L^R \leq 200$	0.0	0.0
$\varepsilon^R/\varepsilon_L^R > 0$, and increases	−0.0933	0.0912	−1.30	$\varepsilon_L^R > 200$	1.246	−247.1
$\varepsilon^R/\varepsilon_L^R > 0$, and decreases	0.1573	−0.1653	−1.00	-	-	-
$\varepsilon^R/\varepsilon_L^R < 0$, and increases	−0.6945	0.5713	−0.63	-	-	-

$$G = G_0 + G_1 \left| \frac{\varepsilon^R}{\varepsilon_L^R} \right|^{G_2(\varepsilon_0^R)} \tag{21}$$

The regression coefficients, G_0 and G_1, are summarized in Table 2. Since the size of the stress-pseudo strain hysteresis loop is dependent upon the amplitudes of pseudo strain incurred in the specimens, the exponent G_2 in Eq. (21) is function of ε_0^R instead of constant values.

All the values of G_2 at different strain amplitudes were obtained from the regression analysis on the experimental data. Since there were four values of G_2 depending on the loading zone for one strain-amplitude data, they were normalized through division by a reference value of G_2, denoted by G_{2R}, for each loading zone. The value of G_2 at the strain amplitude of 0.0014 unit in Table 2 was selected as the G_{2R} value. The normalized G_2 values were then plotted against ε_0^R in Fig. 7. As shown in this figure, it was desirable to have some more data near the origin to obtain regression curves because only two strain-amplitude data were available. As discussed earlier, there was no stress-pseudo strain hysteresis loop developed (i.e., G_2=0) when the damage was negligible (i.e., in a linear viscoelastic range). Therefore, from the study of monotonic loading data, the ε_0^R value of 200 was assumed as an upper limit of this linear viscoelastic range. The regression analysis on the data shown in the figure resulted in the following form:

$$G_2(\varepsilon_0^R) = G_{2R}\left[\beta_0 + \frac{\beta_1}{\varepsilon_0^R}\right] \tag{22}$$

The regression coefficients in Eq. (22) are summarized in Table 2.

6.4. Uniaxial viscoelastic constitutive model under the controlled-stress mode

Before the controlled-strain constitutive Eq. (19) is applied to the controlled-stress mode, a careful investigation was made on the controlled-stress fatigue test data to identify the basic difference in hysteretic behavior and damage growth under both modes of loading. Fig. 8 presents a typical pseudo stress-strain relationship. It can be seen from Fig. 8 that the pseudo stiffness σ^R/ε decreases as cyclic loading continues. Unlike the controlled-strain case, negligible hysteresis loop is observed in the controlled-stress mode.

Using the controlled-stress fatigue test data, the S_p values were calculated from Eq. (6) with p= $2(1+1/m)$. Different from the controlled-strain case, S_p was not able to eliminate the stress level dependency. Therefore, $p=2/m$ was attempted and successfully handled the stress level

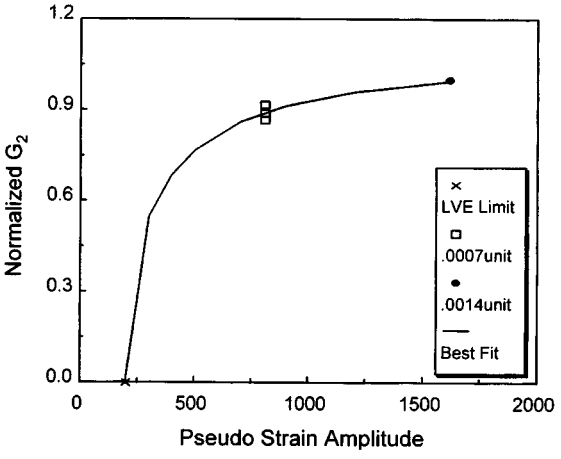

Fig. 7 Normalized G_2 versus ε_0^R

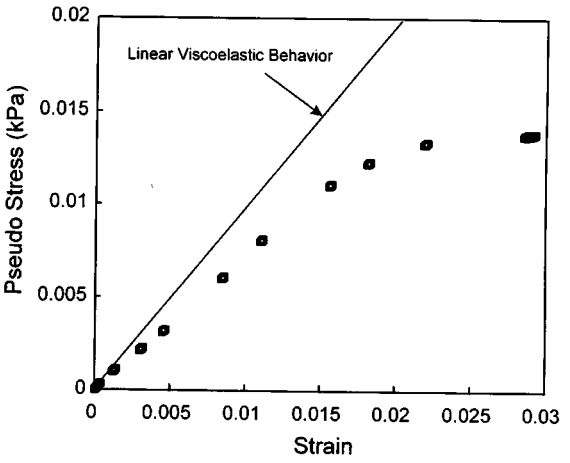

Fig. 8 Pseudo stress-strain behavior of asphalt concrete under controlled-stress cyclic loading

dependency as shown in Fig. 9(a). These observations suggest that $k=(1+1/m)$ is a better assumption for the controlled-strain mode while $k=1/m$ is adequate for the controlled-stress case. Based on the theoretical relationship between the failure zone characteristics and k value discussed in the section *Damage Parameter*, it is possible to speculate that the material's fracture energy (Γ) and failure stress are constant under the controlled-strain mode while the fracture process zone size and Γ are constant under the controlled-stress mode (Lee and Kim 1997).

Since the reduction in S^R was observed from both modes of loading, the characteristics of S^R-S_p relationship were compared in Fig. 9(a). It is observed from this figure that the S_p value of the controlled-strain mode is larger than the one of the controlled-stress mode for a given value of S^R. This discrepancy may be attributed to several factors. In the controlled-strain fatigue tests, both tensile (a positive sign) and compressive (a negative sign) stresses occur in a specimen, while only tensile stresses occur in the specimen under the controlled-stress mode. Schapery (1981) proposed the damage parameter in terms of $|\varepsilon^R|$ instead of ε^R to include some damage due to the compressive stresses. However, most of the cracks observed during the controlled-strain fatigue tests conducted in this study were tensile cracks, which propagated in the direction perpendicular to the loading direction. This implies that the compressive stresses caused little damage to the specimen. Furthermore, the compressive stresses have beneficial effects on the closing of tensile cracks. Therefore, the use of $|\varepsilon^R|$ in the controlled-strain mode may result in the overestimation of the damage.

For the above reasons, S_p was normalized by using a value of S_p at failure, denoted by S_f. To determine the value of S_f, the failure criterion of a specimen should be established a priori. The most common failure criterion of asphalt concrete under the controlled-strain mode is a 50 percent reduction in the initial stiffness (Yoder and Witczak 1975). Knowing the stiffness reduction is due to both relaxation and damage growth of the materials, this failure criterion is modified to the 50 percent reduction in the *initial pseudo stiffness* to eliminate the viscoelasticity of the materials. Then, the value of S_f is the one corresponding to the 50 percent of the initial secant pseudo stiffness as shown in Fig. 9(a). In the controlled-strain mode, the S_f value was 1,900, and in the controlled-stress mode, 760. *The normalized damage parameter* S_n is defined

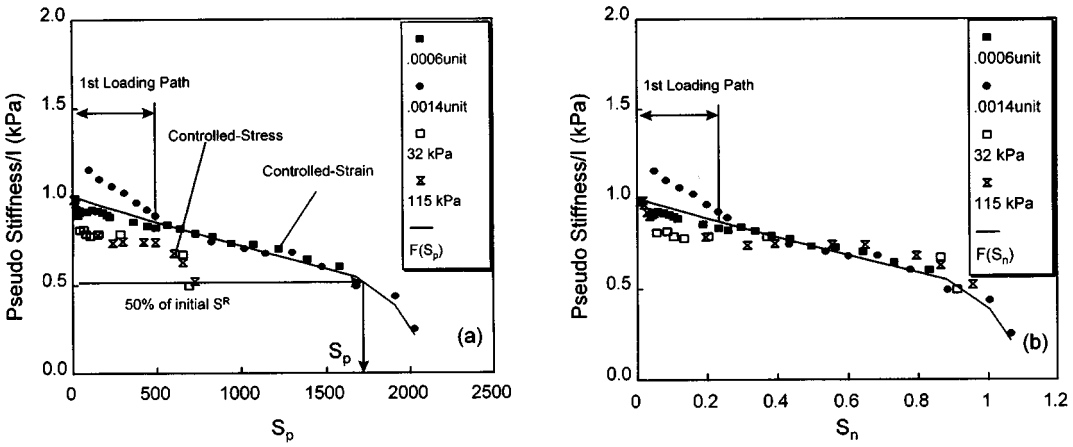

Fig. 9 Reduction in S^R under both modes of loading: (a) S^R vs S_p; (b) S^R vs S_n

as follows:

$$S_n = \frac{S_p}{S_f} \tag{23}$$

The S_p in Eq. (20) is then replaced with S_n:

$$F(S_n) = F_0 - F_1(S_f S_n)^{F_2} \tag{24}$$

The S^R values shown in Fig. 9(a) were plotted against the S_n values in Fig. 9(b). As can be seen in this figure, all the S^R values for both modes of loading fall on the same curve except at the first loading path.

To take advantage of the constitutive relationship developed from the controlled-strain tests, the constitutive Eq. (19) is transformed to account for the controlled-stress case. That is, the physical stress and pseudo strain in Eq. (15) are replaced with pseudo stress and physical strain as follows:

$$\sigma^R = I(\varepsilon)\left[F(S_n) + G\left(\varepsilon_0, \frac{\varepsilon}{\varepsilon_L}\right)\right] \tag{25}$$

where ε_L is the largest value of strain up to current time for all cycles. It can be seen from the typical strain response as shown in Fig. 11(a) that the values of $\varepsilon/\varepsilon_L$ are mostly larger than 0.6. Thus, as can be seen in Fig. 6(b), $G \approx 0$ when $\varepsilon/\varepsilon_L > 0.6$. Then, Eq. (25) may be reduced to

$$\varepsilon = \frac{\sigma^R}{IF(S_n)} \tag{26}$$

Except that pseudo stress is employed in Eq. (26) instead of pseudo strain, one of the major differences between the controlled-strain and -stress constitutive equations is that the hysteresis function G, which accounts for the hysteretic behavior of stress-pseudo strain, is not needed in the controlled-stress case. This can be proved by the $\sigma^R - \varepsilon$ behavior shown in Fig. 8. There is no significant hysteresis loop observed in this figure that supports the validity of the constitutive Eq. (26). Now, one may predict strain response for sinusoidal stress input from Eq. (26) using pseudo

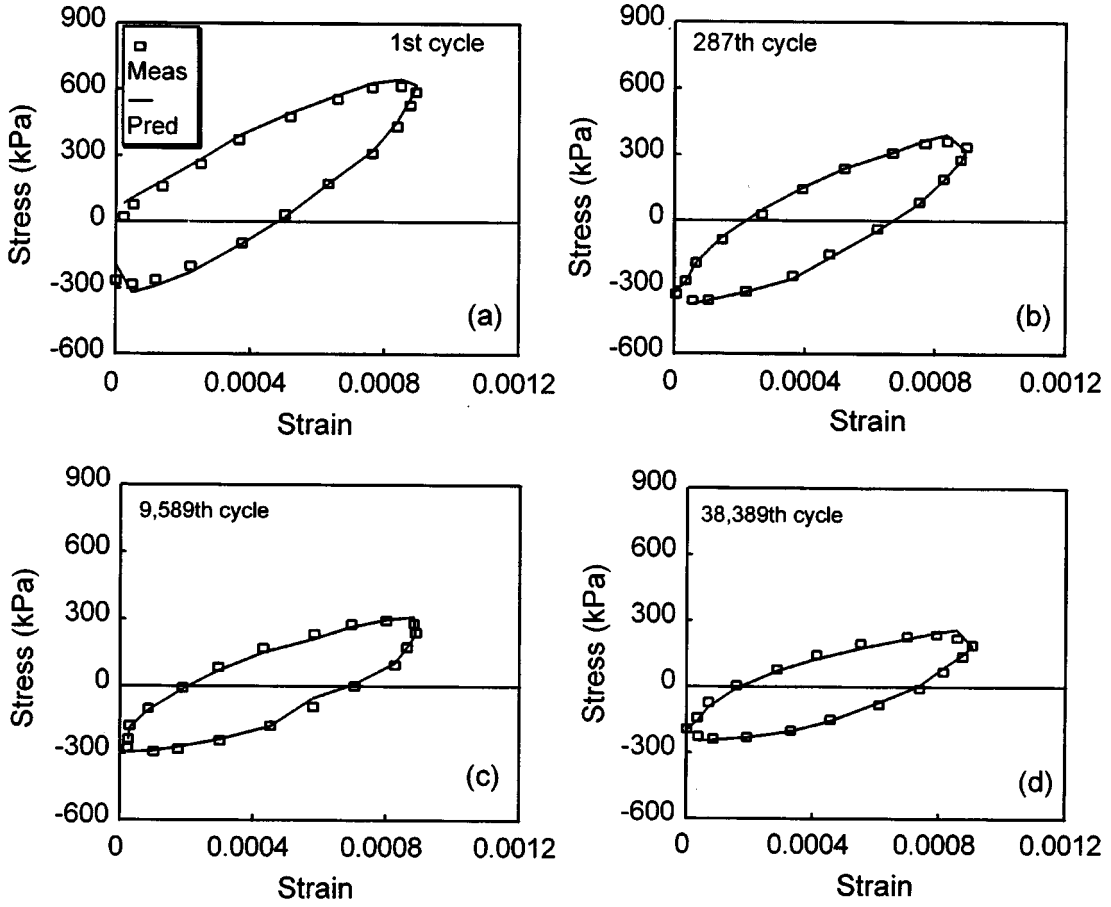

Fig. 10 Validation of the constitutive model under the controlled-strain mode with the strain amplitude of 0.0009 unit (N_f=44,000)

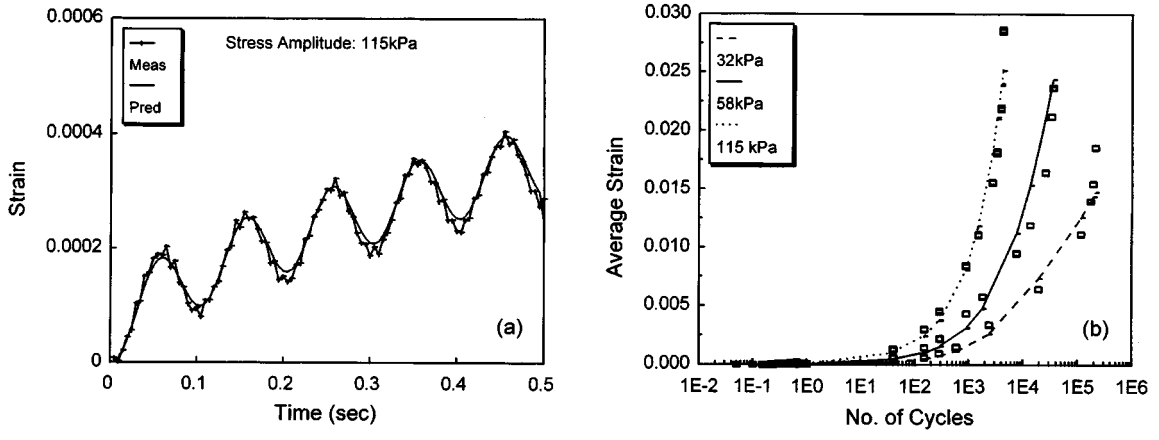

Fig. 11 Validation of the constitutive model under the controlled-stress mode with various stress amplitudes: (a) prediction of strain in the first 5 cycles; (b) prediction of average strain histories up to failure

stress obtained from Eq. (14) and damage function F obtained from the controlled-strain cyclic test data.

7. Validation of the constitutive model

For the verification purposes, two types of uniaxial testing were performed at 25°C:

1. Controlled-strain fatigue test with the strain amplitudes of 0.0009 unit; and
2. Controlled-stress fatigue tests with various stress amplitudes.

Fig. 10 demonstrates the verification of the model for the controlled-strain fatigue tests. To validate the constitutive model for entire fatigue life of asphalt concrete, 4 cycles were randomly selected for presentation, which represent initial, early, intermediate, and final states of fatigue life of the specimens. Fig. 11 represents the validation results of the controlled-stress constitutive model. In general, an excellent agreement is found between the measured and predicted values.

In Fig. 10, the constitutive model successfully predicts the reduction in stresses in the controlled-strain test all the way up to failure. Since the strain amplitude used in the verification test was not used in the determination of the coefficients in the constitutive Eq. (19), it is proved again that S_p is an excellent means of eliminating the strain-level-dependence of the materials.

In Fig. 11, the accuracy of prediction in the controlled-stress fatigue test is not as good as the prediction in the controlled-strain case. It must be noted here that the coefficients in Eq. (26) used in the prediction were obtained from the controlled-strain fatigue tests. The extrapolation from the controlled-strain mode to the controlled-stress mode might have affected the accuracy. Although the prediction is not as good as the controlled-strain case, the constitutive model reasonably predicts the increase in strain up to failure, indicating the validity of the constitutive model in Eq. (26).

8. Conclusions

Damage accumulation under uniaxial tensile cyclic loading without rest periods was modeled using the elastic-viscoelastic correspondence principle and the time-dependent damage parameter. The pseudo variables greatly simplified the task of separately evaluating viscoelastic behavior and damage growth of asphalt concrete. The damage parameter successfully eliminated stress/strain-level-dependence of asphalt concrete on fatigue behavior. The constitutive Eq. (19) developed for the controlled-strain mode was easily transformed to the controlled-stress constitutive Eq. (26) by simply replacing the σ and ε^R with σ^R and ε. The constitutive Eq. (19) and (26) satisfactorily predicted the stress-strain behavior of asphalt concrete all the way up to failure under the controlled-strain and -stress modes, respectively.

References

Chan, S.Y.N., Dhir, R.K., Hewlett, P.C. and Chang, D.Y. (1994), "Near surface characteristics of concrete prediction of freeze/thaw resistance", *Structural Engineering and Mechanics, An Int. J.*, **2**(4), 403-412.

Kim, Y.R. and Little, D.N. (1990), "One-dimensional constitutive modeling of asphalt concrete", *Journal of Engineering Mechanics, ASCE,* **116**(4), 751-772.

Kim, Y.R., Lee, Y. and Lee, H.J. (1995), "Correspondence principle for characterization of asphalt concrete", *Journal of Materials in Civil Engineering, ASCE,* **7**(1), 59-68.

Lee, H.J. (1996), "Uniaxial constitutive modeling of asphalt concrete using viscoelasticity and continuum damage theory", Ph.D. Dissertation, Department of Civil Engineering, North Carolina State University, Raleigh, NC.

Lee, H.J. and Kim, Y.R. (1997), "A viscoelastic constitutive model of asphalt concrete under cyclic loading", *Journal of Engineering Mechanics, ASCE* (in Press).

Mattos, H.S.C. and Sampaio, R. (1995), "Analysis of the fracture of brittle elastic materials using a continuum damage model", *Structural Engineering and Mechanics, An. Int. J.,* **3**(5), 411-427.

Reddy, J.N. and Rasmussen, M.L. (1982), *Advanced Engineering Analysis*, John Wiley & Sons, 203-205.

Schapery, R.A. (1981), "On viscoelastic deformation and failure behavior of composite materials with distributed flaws", *1981 Advances in Aerospace Structures and Materials* (eds., Wang, S.S. and Renton, W.J.), *ASME*, AD-01, 5-20.

Schapery, R.A. (1984), "Correspondence principles and a generalized J-integral for large deformation and fracture analysis of viscoelastic media", *International Journal of Fracture Mechanics,* **25**, 195-223.

Yoder, E.J. and Witczak, M.W. (1975), *Principles of Pavement Design*, John Wiley & Sons, 284-285.